Available online at www.sciencedirect.com
ScienceDirect
International Journal of Thermal Sciences 47 (2008) 1544–1554
International Journal of Thermal Sciences
www.elsevier.com/locate/ijts

Effect of vane/blade relative position on heat transfer characteristics in a stationary turbine blade: Part 2. Blade surface

Dong-Ho Rhee [a], Hyung Hee Cho [b,*]

[a] *Korea Aerospace Research Institute, Daejeon 305-333, Republic of Korea*
[b] *Department of Mechanical Engineering, Yonsei University, Seoul 120-749, Republic of Korea*

Received 10 November 2006; received in revised form 5 September 2007; accepted 12 December 2007

Available online 18 January 2008

Abstract

This study was carried out to investigate local heat/mass transfer characteristics on the stationary blade near-tip surface for various relative positions of the blade. A low speed wind tunnel with a stationary annular turbine cascade was used. The test section has a single turbine stage composed of sixteen guide plates and sixteen blades. The chord length of the blade is 150 mm and the mean tip clearance of the blade is 2.5% of the blade chord. Detailed mass transfer measurements were conducted for the stationary blade fixed at six different relative blade positions in a single pitch using a naphthalene sublimation method. The Reynolds number based on the blade inlet velocity and the chord length ranges between 1.0×10^5 and 2.3×10^5 and mean turbulence intensity is about 3%. The change in blade position, which causes a different interaction between vane and blade, changes the incoming flow condition. As a result, significantly different patterns are observed on the blade surface, especially near the blade tip due to the variation in tip leakage flow.

Keywords: Turbine blade; Near-tip surface; Tip leakage flow; Heat/mass transfer; Relative position; Naphthalene sublimation method

1. Introduction

The near-tip region and the tip surface of the turbine blade are typical regions subject to an excessive thermal load since the turbine blade tip operates in an extremely high temperature environment with complex flow fields. Since the turbine blade has a finite tip clearance between the tip and the shroud, leakage flow is generated through the clearance by the pressure differential between the pressure and suction sides of the blade. Due to the leakage flow through the gap, extremely high heat transfer rates are observed near the tip and on the tip of the blade. Also, the leakage flow discharged from the tip gap interacts with the mainstream (hot gases) near the suction side tip of the blade, which causes excessive heat transfer on the surface. Therefore, the region around the blade tip needs to be protected by intensive cooling because the tip and near-tip regions are difficult to cool effectively due to their complicated geometry and flow patterns. To improve the reliability and durability of the turbine blade, complex cooling techniques should be developed and used at the tip and near-tip regions. An accurate understanding of detailed heat transfer characteristics is required to develop more effective cooling techniques.

Many researchers have dealt with heat transfer characteristics on the blade or vane, especially in the mid-span (two-dimensional flow region) and endwall [1–8]. Moreover, as reviewed in Part 1 [9], most of the studies on blade heat transfer around the tip focus on the blade tip. Although the blade near-tip region is one of the weak regions exposed to severe operating conditions, only limited information on near-tip heat transfer has been provided by a few researchers. Kwak and Han [10] measured detailed heat transfer coefficients on the near-tip surface, tip and shroud in a stationary linear turbine cascade using a transient TLC (thermochronic liquid crystal) measurement technique. Jin and Goldstein [11] conducted experiments to investigate the local heat transfer characteristics on the near-tip surface for a low speed stationary linear turbine cascade using a naphthalene sublimation method. In their study, complex distributions of mass transfer coefficients are observed

* Corresponding author. Tel.: +82 2 2123 2828; fax: +82 2 312 2159.
E-mail address: hhcho@yonsei.ac.kr (H.H. Cho).

1290-0729/$ – see front matter
doi:10.1016/j.ijthermalsci.2007.12.007

Nomenclature

C	blade chord length
C_P	static pressure coefficient
C_x	blade axial chord length
D_{naph}	diffusion coefficient of naphthalene in the air
h_m	local mass transfer coefficient
l	blade span
p	blade pitch
P_0	total pressure of incoming flow
P_s	static pressure on blade surface or shroud
Re_C	Reynolds number based on blade chord length and incoming flow velocity
$Re_{C,ex}$	Reynolds number based on blade chord length and exit flow velocity
S	spacing between guide plate and blade
Sh_C	Sherwood number based on blade chord length
t	tip clearance
Tu	turbulence intensity of incoming flow
U	flow velocity at the vane exit
U_{mean}	average flow velocity at the guide plate exit
V_0	mean flow velocity at the inlet of guide plate
W_1	mean flow velocity at the blade inlet
W_2	mean flow velocity at the blade exit
x, y, z, s	coordinate system (Fig. 2)

Greek symbol

α_1	guide plate exit angle
α_2	absolute flow angle at the blade exit
β_1	blade inlet angle
β_2	blade exit angle

due to the passage and tip leakage vortices. Kwon et al. [12] also reported the effect of tip leakage flow on blade surface heat transfer. Recently, Rhee and Cho [13] investigated blade near-tip heat transfer using a naphthalene sublimation method and provided detailed heat/mass transfer information on the rotating blade under various conditions.

In addition, most studies have dealt with heat or mass transfer on the blade for uniform incoming flow. However, in actual operating conditions, the flow field around the blade is non-uniform and unsteady due to various effects such as vane/blade interaction, wake and blade rotation which can cause different heat transfer characteristics. Therefore, various parameters and operating conditions should be taken into account.

Giel et al. [8] studied the effect of incidence angle on the blade surface in a transonic linear turbine cascade without tip clearance. They changed the incidence angle from −5 deg. to 5 deg. and reported a significant change in the heat transfer pattern with a non-zero incidence angle. Rhee and Cho [14,15] investigated the effect of incidence angle for a rotating turbine blade in a low speed wind tunnel and also demonstrated considerable variation in the heat transfer coefficient in the near-tip region. Zhang and Han [16], Du et al. [17] and Rhee and Cho [18] investigated the effect of upstream wake on blade surface heat transfer and reported that the upstream wake elevates the heat transfer coefficient in the general region of the blade.

The present study focused on the effects of vane/blade interaction, particularly, the effect of blade position with respect to the upstream vane. Part 1 [9] dealt with the tip and shroud heat/mass transfer and the present paper focuses on heat/mass transfer in the near-tip region of the blade. The relative blade position changes the opening area of the upstream vane and results in periodic variation of flow and heat transfer characteristics around the blade tip. To estimate the effect of vane/blade interaction, a set of experiments was conducted for a stationary blade with six different positions with respect to the upstream guide plate. In the experiment, a low speed wind tunnel with a stationary annular turbine cascade was used and a row of guide plates was installed in front of the stationary blade. A blade with flat tip geometry was used and detailed mass transfer measurements of the tip, shroud and blade near-tip surface were conducted using a naphthalene sublimation method. To investigate the effect of vane/blade interaction, at first, basic heat transfer characteristics were examined for a uniform incoming flow condition and then the experiments were performed for the blade fixed at various relative positions. In addition, for the condition of uniform incoming flow, the effect of Reynolds number was also investigated. A naphthalene sublimation technique was used to measure detailed mass transfer coefficients on the blade.

2. Experimental facilities

2.1. Wind tunnel with stationary annular cascade

Fig. 1 shows a schematic view of a low speed wind tunnel with an annular turbine cascade. The apparatus is composed of three parts: an upstream fan with 15 HP motor, an annular passage with test section (a single stage of the turbine) and a downstream fan with 10 HP motor. The outer and inner diameters of the annular passage are 900 and 620 mm, respectively, and the corresponding height of the passage is 130 mm. The annular passage has a 1.7 m-long straight section based on the outer casing. The details of the apparatus are described in Part 1.

The test section of a single turbine stage is located in the annular passage (Fig. 2). To simulate a single stage turbine, the test section has a row of sixteen guide plates and a row of sixteen turbine blades. The guide plate is located 540 mm downstream of the inlet of the passage. The guide plates are made of steel plate. The axial chord length of the guide plate is 120 mm and each guide plate has a 56.4 deg.-exit angle. The geometry of the guide plates is given in Table 1. A row of turbine blades is located 34 mm downstream of the guide plate.

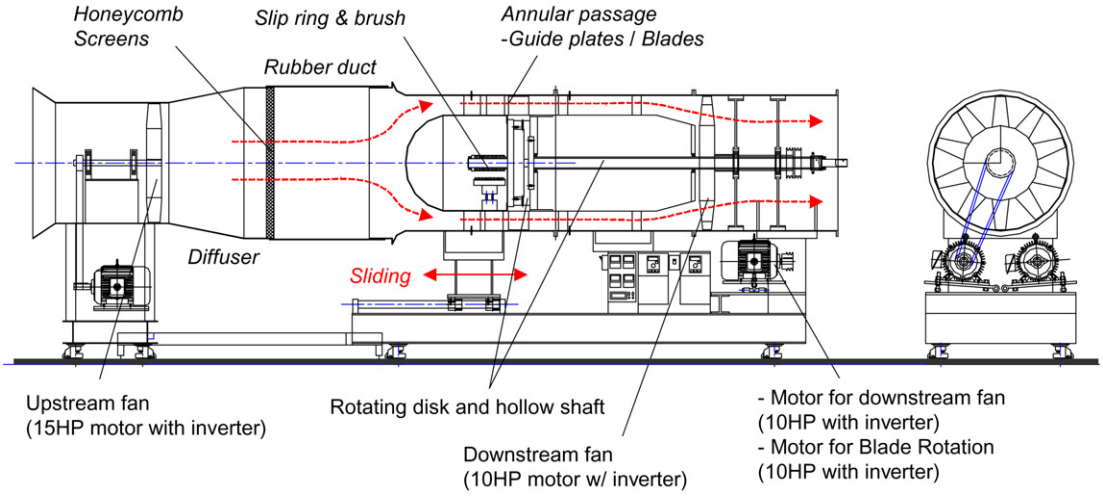

Fig. 1. Schematic view of experimental facility.

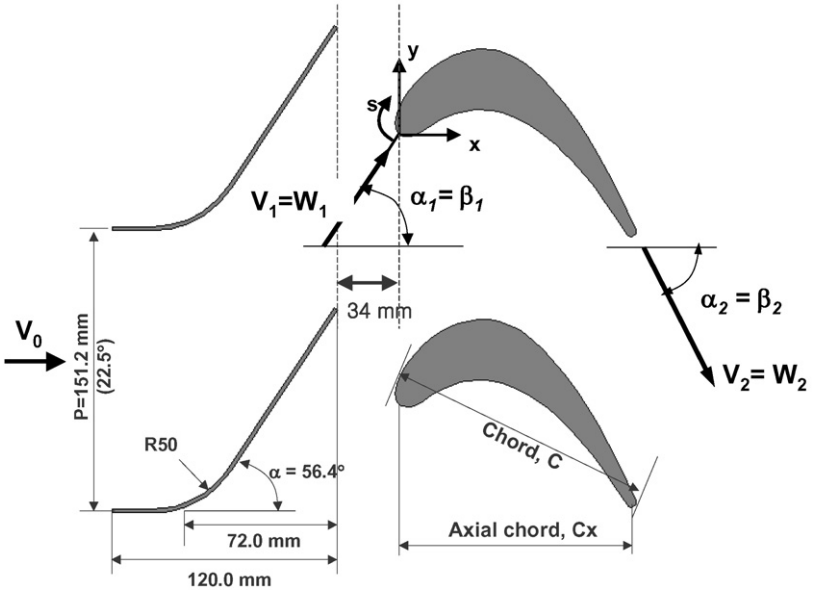

Fig. 2. Schematic view of guide vane and blade.

Table 1
Guide plate configurations

Number of guide plates	16
Axial chord length (C_x)	120 mm
Pitch	22.5° ($P/C = 1.26$)
Aspect ratio (l/C)	1.08
Guide plate inlet/exit angle	0°/56.4°

Table 2
Blade configurations

Number of blades	16	
Chord length (C)	150 mm	
Axial chord (C_x)	131.5 mm	
Pitch to chord ratio (p/C)	Hub	0.84
	Mean	1.01 (22.5°)
	Tip	1.17
Aspect ratio (l/C)	0.87	
Spacing between vane and blade	34 mm (0.227C)	
Blade inlet/exit angle	$\beta_1 = 56.4°/\beta_2 = -62.6°$	
Turning angle	119.0°	
Mean tip clearance (t)	3.8 mm ($t/C = 2.5\%$)	

The mid-span profile of a GE 7FA first stage blade was used for the turbine blade. The chord length of the blade is 150 mm and the corresponding aspect ratio is 0.87. The nomenclature and details of the blade geometry are given in Fig. 2 and Table 2.

Two pitot tubes and six J-type thermocouples were located 100 mm upstream from the guide inlet to measure the velocity and temperature of the incoming flow. For the flow measurement at the inlet of the blade, a constant temperature thermal anemometer (IFA-300 from TSI, Inc.) with single hot-film probe (Model 1201-6) was used. Several windows were made on the outer casing for local mass transfer measurements and flow/static pressure measurements on the shroud. Several curvilinear test plates made of acrylic were used for velocity and static pressure measurements.

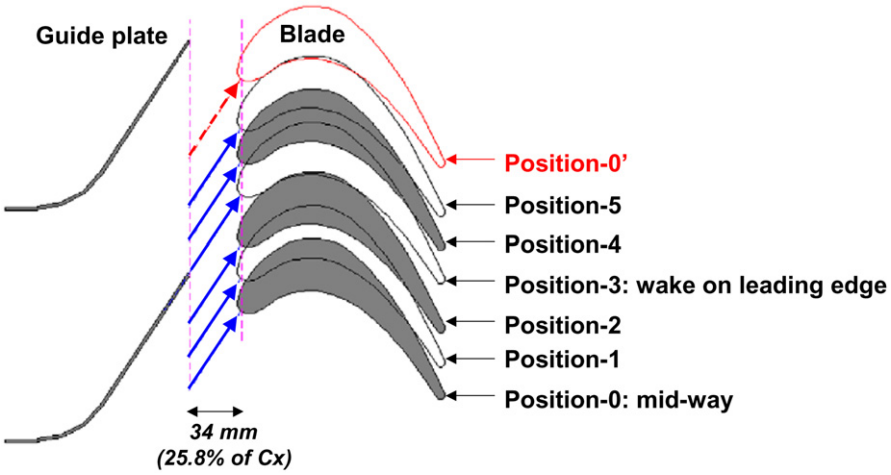

Fig. 3. Schematic of various relative positions of stationary blade.

Table 3
Operating condition

Guide inlet flow velocity (V_0)/mean Tu	8.3 m/s/∼9%
Guide exit flow velocity (V_1)*	24.3 m/s
Blade inlet velocity (W_1)/mean Tu	15 m/s/∼3%
Blade exit velocity (W_2)*	18.0 m/s
Reynolds number based on W_1 and C ($\mathrm{Re_C}$)	1.5×10^5
Reynolds number based on W_2 and C ($\mathrm{Re_{C;exit}}$)	1.5×10^5

(based on mid-span geometry and the inlet Reynolds number). *: calculated from inlet to exit area ratio.

2.2. Relative position of blade and operating conditions

As mentioned in Part 1 (reference), to investigate the effect of relative blade position, the experiments were conducted for the stationary blade fixed at six different positions. Fig. 3 shows the schematic view of the blade positions at the mid-span. Position 0 (or Position 0′) means that the blade is located at the midpoint of the passage while Position 3 means that the extended line from the guide trailing edge is coincident with the blade leading edge. Positions 1 and 2 indicate the blade positions 0.15C apart from Positions 0 and 1, respectively in the pitchwise direction. Similarly, Positions 4 and 5 represent the positions 0.15C apart from Positions 3 and 4, respectively, in the pitchwise direction. Thus, a single pitch may be resolved into six positions and the effect of blade position on local heat/mass transfer may be investigated.

The experiments were conducted at an inlet Reynolds number ($\mathrm{Re_C}$) of 1.5×10^5. The mean velocity at the blade inlet is 15 m/s and the turbulence intensity is about 3%. The boundary layer thickness on the casing is less than 5 mm. All experiments were conducted at room temperature and the variation in room temperature during the experiments was maintained within ±0.3 °C. Details of the operating conditions are listed in Table 3.

3. Mass transfer measurement and data reduction

Detailed mass transfer measurements were conducted on the blade surface using a naphthalene sublimation method. The present study focused on local heat/mass transfer on the near-tip region so the test blade was designed to have a naphthalene-coated surface from 15 mm below the mid-span to the near-tip region (4 mm below the tip). The test blade surface has a rim of 4 mm along the blade tip to maintain the sharp edge of the blade tip and to provide the reference value for sublimation depth measurement.

In the results, the Sherwood number is used as a dimensionless form of mass transfer coefficient and the Sherwood number is expressed as:

$$\mathrm{Sh_C} = h_m C / D_{\mathrm{naph}} \tag{1}$$

where D_{naph} is calculated from a correlation equation suggested by Goldstein and Cho [19]. Uncertainty in Sherwood numbers using the method of Kline and McClinetock [20] for single sample experiments was estimated to be ±7.4% in the entire operating range of the measurement, based on a 95% confidence interval. Mass transfer coefficients can be converted into heat transfer coefficients using the heat and mass transfer analogy [21] and the comparison results for blade surface heat transfer are given by Rhee and Cho [14].

4. Results and discussion

4.1. Static pressure measurements

Fig. 4 shows the distributions of time-averaged static pressure coefficients ($C_p = (P_s - P_0)/0.5\rho V_0^2$) at the mid-span for Position 5. It should be noted that the static pressure measurements were conducted for Position 5 because it has a more uniform distribution of velocity magnitude than other cases as mentioned in Part 1 [13]. In the figure, the bold line indicates the result from a 3D numerical simulation using FLUENT 6.1 and the open symbols represent the experimental data. The simulation was performed to obtain steady solutions for a turbulent viscous flow field around the blade tip. The model geometry and the operating conditions are the same as the experimental ones. A guide plate and a blade were modeled and a periodic boundary condition was imposed on the sidewalls. The grid was generated by GAMBIT solid modeling and the number of cells

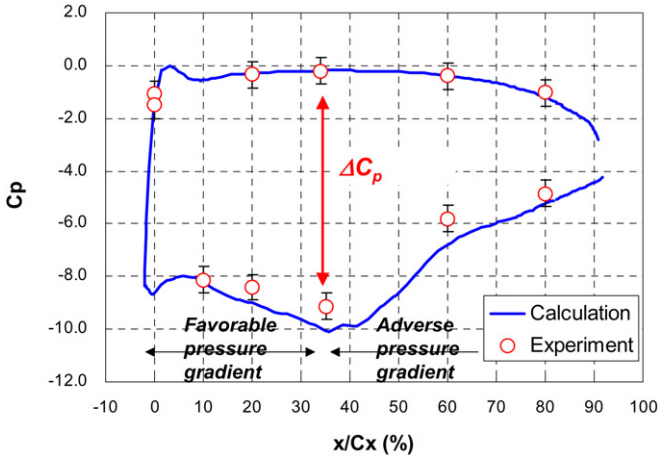

Fig. 4. Static pressure distribution at mid-span.

was about 1.5 million. The RNG k–ε turbulence model with non-equilibrium wall function was used.

As shown in Fig. 4, while C_p values on the pressure side are uniform, on the suction side surface, C_p decreases considerably with flow acceleration. The maximum static pressure difference is observed at $x/C_x \cong 0.34$ and then the static pressure recovers forming an adverse pressure gradient. The numerical simulation predicts a minimum value at $x/C_x \cong 0.1$ on the pressure side, and a laminar separation bubble may be formed near this region.

4.2. Heat/mass transfer characteristics with uniform incoming flow

Fig. 5 shows the contour and local plot of Sh_C on the blade surface for the stationary blade at $Re_C = 1.5 \times 10^5$. In the contour plot, the dashed line indicates the mid-span of the blade and the outer-lines of the contour plot indicate the blade surface. The regions in which the mass transfer coefficient is not measured, such as the rim near the tip and trailing edge, are excluded from the result.

The flow characteristics primarily affecting local heat transfer on the blade surface near-tip region are classified as follows and indicated in Fig. 6(a). The highest values of Sh are observed along the span at the leading edge (stagnation region, Region I in Fig. 6(a)) and then Sh decreases as the flow develops on the surface. On the pressure side ($s/C_x \leqslant 0.0$), the flow after the stagnation point is expected to be laminar due

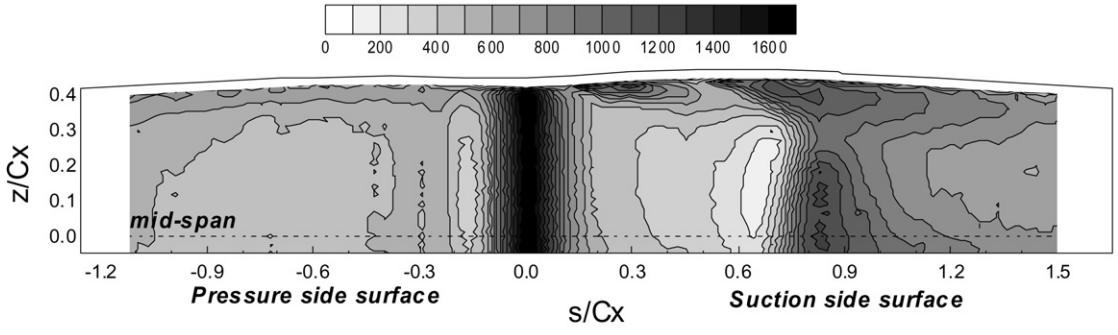

(a) contour plot

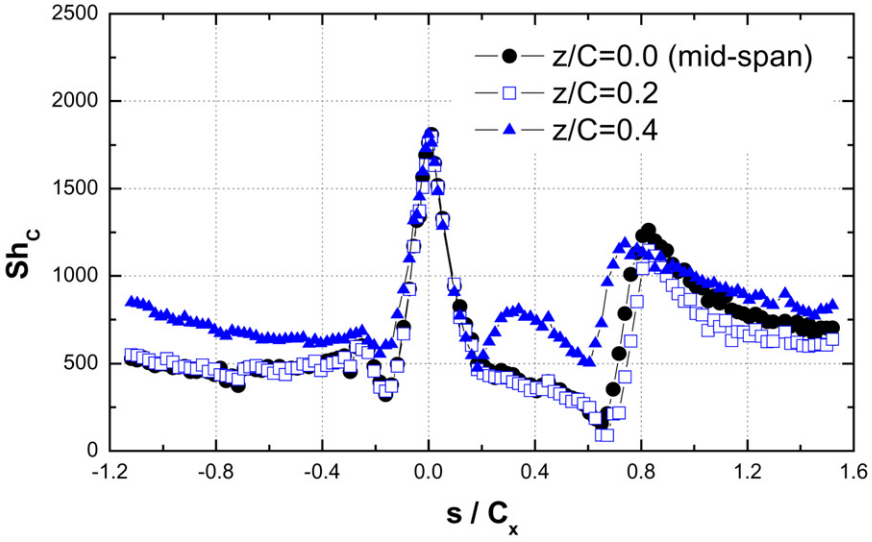

(b) local distributions along the surface

Fig. 5. Local Sh_C on the blade surface for Position 5 at $Re_C = 1.5 \times 10^5$. (a) Contour plot, (b) local distributions along the surface.

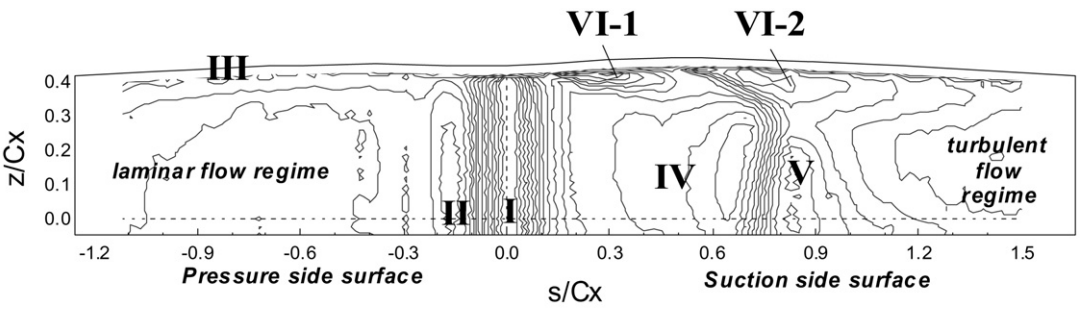

(a) blade surface

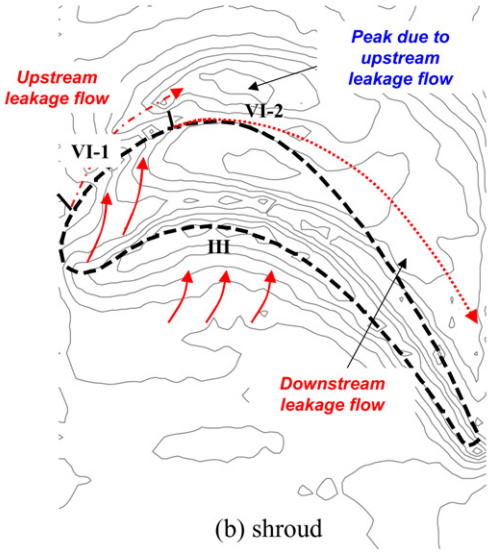

(b) shroud

Fig. 6. Classification of heat transfer characteristics on the blade surface and the shroud. (a) Blade surface, (b) shroud.

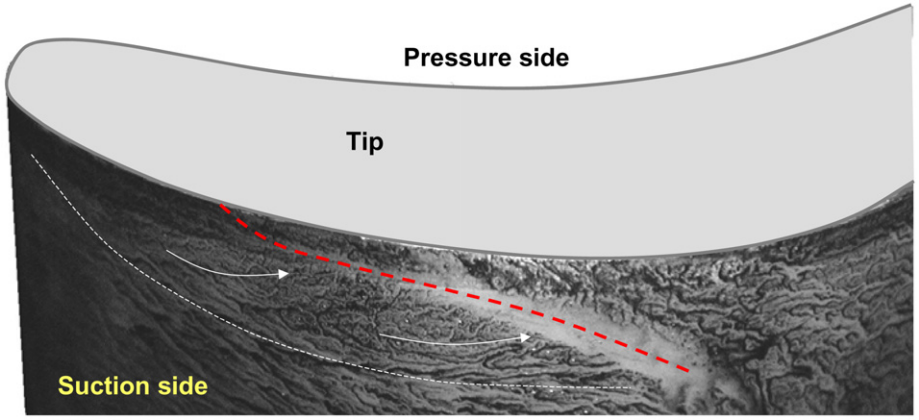

Fig. 7. Oil-lampblack flow visualization on the suction surface of the blade.

to local flow acceleration. As flow moves downstream on the pressure side, local peak and valley are found at $s/C_x \cong -0.2$ due to laminar flow separation (Region II) and flow reattachment on the pressure side surface. After flow reattachment, the heat transfer coefficient decreases rapidly as the boundary layer develops. Then, the boundary layer flow undergoes relaminarization and quite uniform heat/mass transfer distributions are found in the downstream region. Near the tip on the pressure side, high heat/mass transfer coefficients are found along the tip due to the flow acceleration (Region III).

On the suction side surface, in the two-dimensional flow region, the laminar boundary layer flow is maintained up to $s/C_x \cong 0.7$ due to strong acceleration (Region IV). Then, the flow transition occurs due to adverse pressure gradient (Region V) and relatively high peak values (about 70% of Sh at the stagnation point, $s/C_x = 0.0$) are observed in this region. Af-

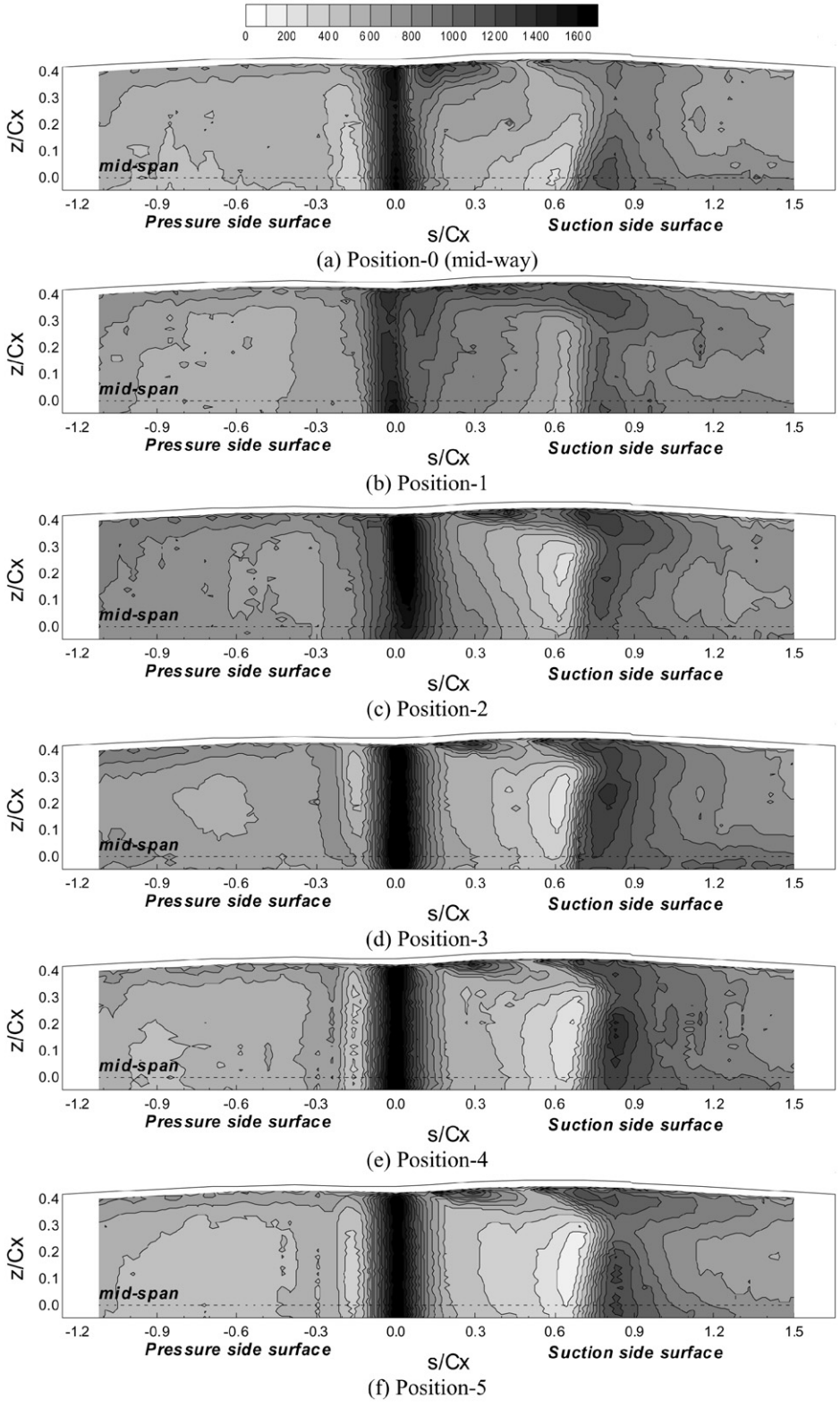

Fig. 8. Contour plots of Sh_C on the blade surface for various positions at $Re_C = 1.5 \times 10^5$. (a) Position 0, (b) Position 1, (c) Position 2, (d) Position 3, (e) Position 4, (f) Position 5.

ter the transition, the fully turbulent boundary layer develops and the heat/mass transfer coefficient decreases monotonically. In the near-tip region of the suction side surface ($z/C_x \geqslant 0.3$), the leakage flow from the gap has a dominant effect on local heat/mass transfer (Region VI). There are two peaks near the tip on the suction side surface, which are indicated as Region VI-1 and Region VI-2 in Fig. 6(a). This is because the leakage flow in the tip gap is divided into upstream and downstream tip leak-

age flows and then these flows develop as two leakage vortices. This feature is explained in Part 1 and can be easily confirmed by comparing with the shroud heat transfer pattern as shown in Fig. 6(b). In the upstream region near the tip (Fig. 6(a)), a small region of high heat/mass transfer is generated due to leakage flow from the upstream portion of the gap. This region is confined to $s/C_x \leqslant 0.4$. This is possibly because the leakage flow affecting the surface heat transfer is detached from the surface as the flow moves along the surface. Then, as indicated in Fig. 6(b), the upstream tip leakage flow begins to affect the shroud heat transfer. Therefore, an additional high heat transfer region is observed on the shroud outside the tip gap.

A new high heat transfer region due to the downstream leakage vortex is observed after a clear demarcation between Regions VI-1 and VI-2 (the local minimum value at $s/C_x = 0.5$ along $z/C_x \cong 0.4$). This tip leakage vortex impinges on the suction side surface, drawing the mainstream (hot gases) toward the surface. Therefore, relatively high heat/mass transfer regions are formed along the leakage vortex path. The effect of the downstream leakage vortex reaches more than 10% of the axial chord in the spanwise direction. As presented in Fig. 5(b), the peak value due to this leakage vortex is located at $s/C_x = 0.7$ and the level is about 60% of that at the stagnation point. The demarcation between Regions VI-1 and VI-2 is shown clearly in the oil-lampblack flow visualization result (Fig. 7).

It should be noted that the horseshoe and passage vortices are negligible in the present study because the boundary layer thickness is equivalent to the tip clearance as mentioned in Part 1.

4.3. *Effect of relative blade position*

Fig. 8 shows the contour plots of Sh_C on the blade surface for various blade positions at $Re_C = 1.5 \times 10^5$. Basically, the local heat/mass transfer characteristics mentioned above are observed for all cases. The level of heat/mass transfer coefficients and the size of the classified regions are different. This change is related to the incoming flow condition variation as presented in Part 1 [13] and the behavior of the tip gap flow.

For Position 0 (Fig. 8(a)), the heat transfer characteristics mentioned above are shown clearly. On the pressure side, the heat transfer coefficients on the pressure side surface are uniform and high heat/mass transfer coefficients are formed near the tip along the pressure side surface. However, some differences from the result at Position 5 (Figs. 5(a) or 8(e)) are found on the suction side surface. On the suction side surface, the heat transfer coefficients in the flow acceleration region ($s/C_x < 0.6$) are slightly higher than those at Position 5 and the locally low transfer regions are reduced. This is possibly due to elevated turbulence intensity of the incoming flow near the suction side surface. Near the tip, the heat transfer enhanced region related to the upstream tip gap flow is larger than that for Position 5. On the contrary, the effect of the tip leakage vortex on the blade surface is weakened. This is due to a reduced downstream tip gap flow with an increased upstream gap flow.

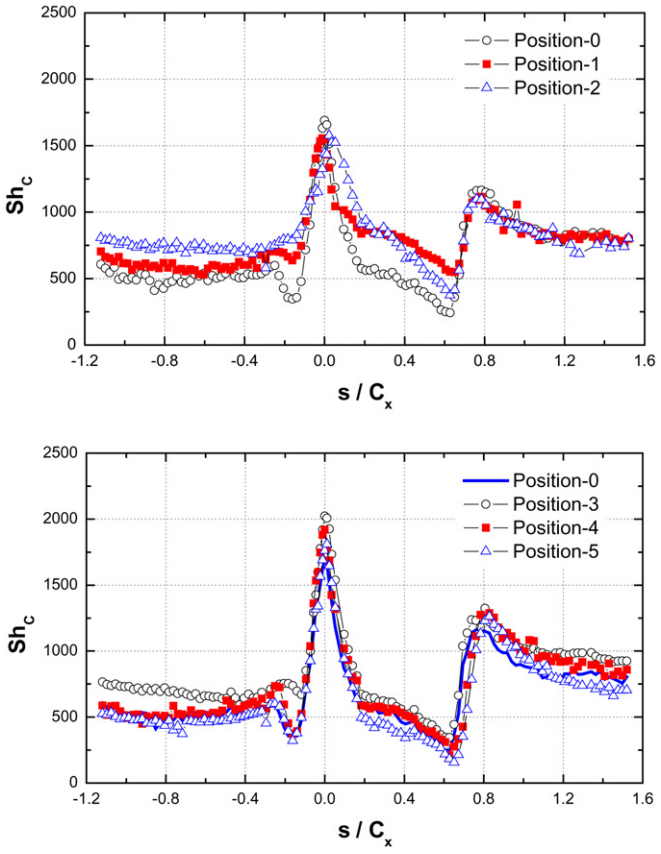

Fig. 9. Local distributions of Sh_C at the mid-span of the blade for various positions at $Re_C = 1.5 \times 10^5$.

This is already mentioned in the shroud heat/mass transfer result (Fig. 6(b)).

For the cases of Positions 1 and 2 (Figs. 8(b) and (c)), significant changes are observed. The region related to the laminar separation bubble on the pressure side surface disappears and the stagnation region is somewhat shifted toward the suction side. Also, heat/mass transfer in the upstream region on the suction side surface is increased due to elevated turbulence intensity. These characteristics are due to low flow velocity with high turbulence intensity of incoming flow around the leading edge, which is presented in Part 1.

Near the tip on the suction side surface, the region of high heat/mass transfer due to the upstream gap flow is significantly reduced while the region affected by the downstream tip leakage vortex is enlarged and the peak value in this region is increased when compared with the case at Position 0 or Position 5. This is due to reduced upstream gap flow with increased downstream tip leakage flow.

At Position 3 (Fig. 8(c)), the wake from the trailing edge of the guide plate directly affects blade leading edge heat transfer. Therefore, the Sh_C values in the stagnation region are higher than those for any other cases. The effect of wake seems to be confined to the stagnation region ($-0.1 < s/C_x < 0.1$) because of local flow acceleration. On the suction side, the high heat/mass transfer region due to the upstream gap flow is larger than that for Position 2, which means the upstream leakage flow begins to increase while the downstream leakage flow is re-

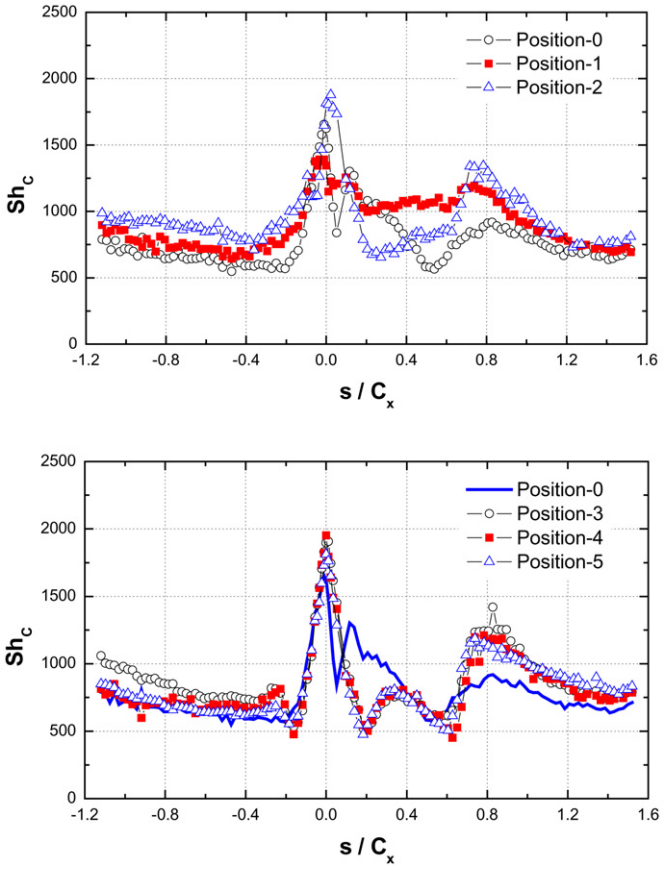

Fig. 10. Local distributions of Sh_C along $z/C_x = 0.4$ of the blade for various positions at $Re_C = 1.5 \times 10^5$.

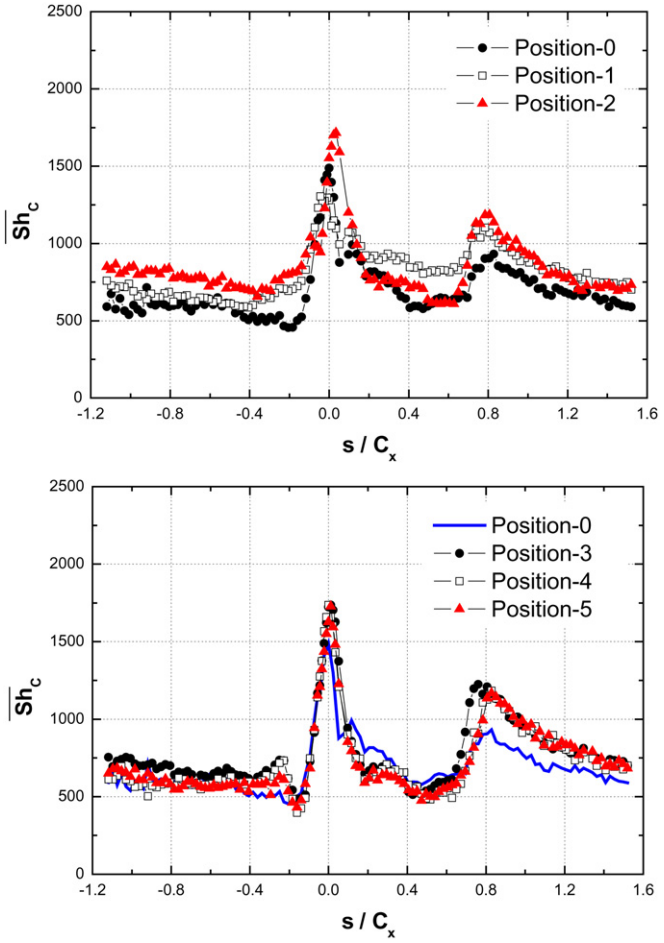

Fig. 11. Distributions of spanwise averaged Sh_C for various blade positions at $Re_C = 1.5 \times 10^5$.

duced as the blade moves from Position 2 to Position 3. While the blade position changes from Position 3 to Position 5, overall heat/mass transfer characteristics are maintained and no significant change is observed.

Looking over the results in series from Position 0 to Position 5 reveals that the effects of leakage flow change with blade position, and consequently local patterns and levels of heat/mass transfer coefficients near the tip change periodically with blade rotation. This means that the near-tip region is exposed to periodically varying heat flux. Therefore, for more accurate heat transfer analysis in the tip region of the blade, not only the uniform flow conditions but also the flow condition induced by vane–blade interaction should be considered.

Figs. 9 and 10 present local distributions of Sherwood number at the mid-span and near the tip for various blade positions. At the mid-span, as mentioned above, different patterns are observed around the stagnation region including the 'flow acceleration region' on the suction side surface for Positions 1 and 2. However, each case has similar heat/mass transfer characteristics and levels of Sherwood number.

Near the tip (Fig. 10), significant change is found on the suction side surface as the blade position changes from Position 1 to Position 3 as shown in the contour plot results. For example, the difference in Sherwood number on the suction side surface is up to 50%. On the contrary, Positions 3, 4 and 5 have quite similar patterns of Sh in the overall region. Therefore, severe variation in heat transfer or thermal load is expected in the near-tip region of the blade when the blade is close to the vane trailing edge.

The distributions of the spanwise averaged Sh_C for various blade positions are presented in Fig. 11. As shown in local distributions, different patterns around the stagnation region and suction side surface are observed for various blade positions. However, the discrepancy is not as much as that in local distribution. Therefore, to understand exact heat/mass transfer characteristics for various operating conditions, detailed measurement and analysis are required.

4.4. *Effect of Reynolds number*

Fig. 12 shows the contour plots of Sh_C on the blade surface at various Reynolds numbers when the blade is fixed at Position 5. As Reynolds number increases, the overall level of heat/mass transfer coefficients also increases while local heat/mass transfer characteristics remain unchanged.

Local distributions of Sherwood numbers normalized by $Re_C^{0.5}$ are presented in Figs. 13 and 14(a). At mid-span, as expected from the contour plots, the distributions are similar in the overall region. Particularly, at tested Reynolds numbers, the position of the flow transition and the separation bubble are not

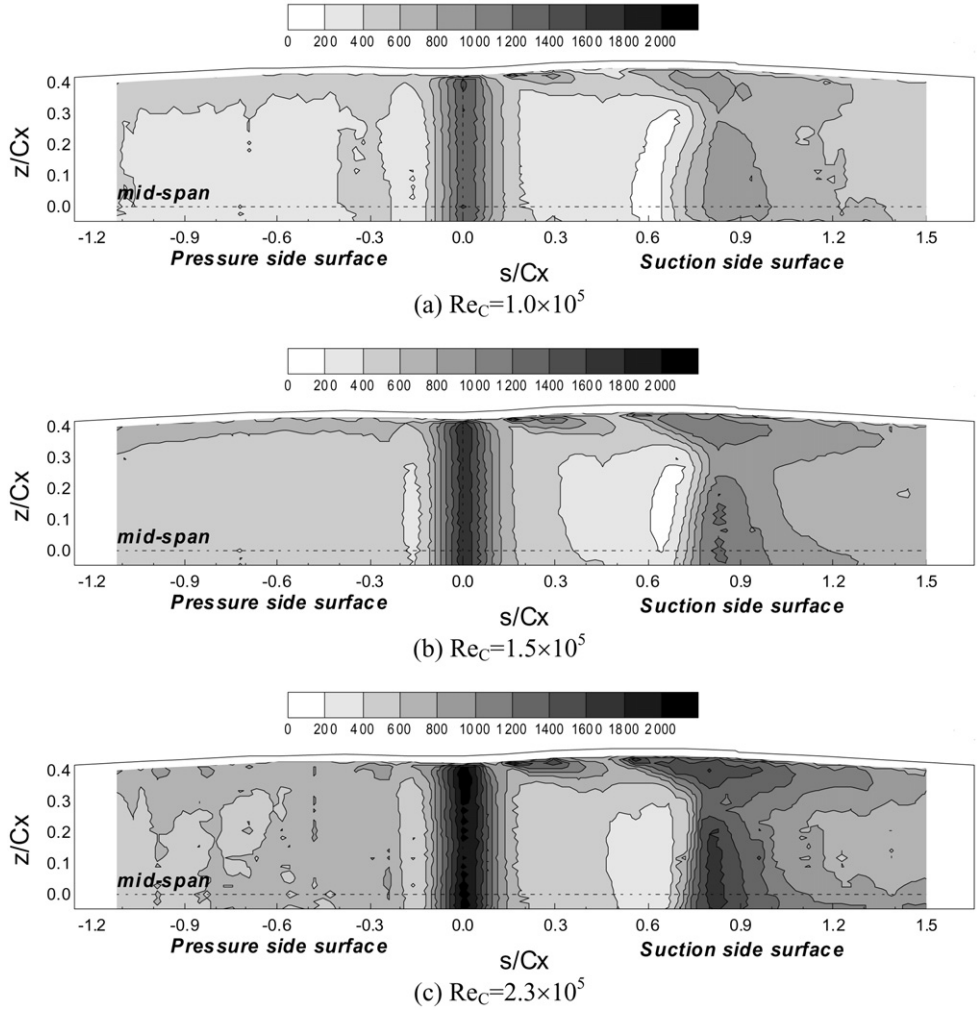

Fig. 12. Contour plots of Sh_C on the blade surface for Position 5 at various Reynolds numbers.

affected. Near the tip (Fig. 14(a)), however, there are some discrepancies in the normalized Sherwood numbers. This means that the flow regime near the tip is fully turbulent and the Sherwood number is not proportional to $Re_C^{0.5}$. Fig. 14(b) presents the Sherwood number normalized by $Re_C^{0.8}$ near the tip on the suction side surface and the normalized values are in quite good agreement. In addition, it should be noted that the flow regime on the surface may be changed and the position of the flow transition also may be shifted or disappear for higher Reynolds numbers, on the order of 10^6.

5. Conclusions

The experimental study was conducted to investigate the effect of the relative position of the stationary blade on blade heat/mass transfer. Detailed heat/mass transfer coefficients were obtained using a naphthalene sublimation method. At first, basic heat/mass transfer patterns with uniform incoming flow were examined on the blade surface and the shroud. Then, the effect of relative position of the blade was investigated for six different blade positions.

The heat/mass transfer characteristics on the blade surface are affected strongly by the local flow characteristics, such as laminarization after flow acceleration, flow transition, separation bubble and tip leakage flow. On the pressure side, local peaks and valley are found due to stagnation, separation bubbles and transition. Also, relatively high heat/mass transfer coefficients are found near the tip due to flow acceleration. On the suction side, complex patterns related to flow acceleration and flow transition are observed in the mid-span region. Near the blade tip, the divided effects of tip leakage flow are shown: upstream and downstream tip leakage flows. The upstream tip leakage flow affects at first the upstream region of the blade near-tip surface and

then it increases the heat/mass transfer rate on the shroud surface. The tip leakage flow in the downstream region mainly has an influence on the blade surface, forming a high heat/mass transfer region in the downstream region of the surface near the tip.

The relative position of the blade changes the incoming flow condition significantly because the opening area varies with the relative position. Therefore, velocity magnitude and turbulence intensity at the blade inlet change significantly with the blade position. As a result, the heat transfer on the surface and shroud is changed with relative position. The maximum difference of Sh_C is up to 30% of the average value in the mid-span region

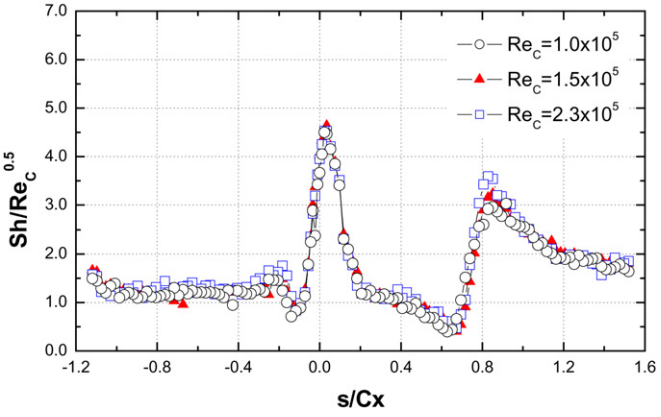

Fig. 13. Local distributions of normalized Sh_C at mid-span for Position 5 at various Reynolds numbers.

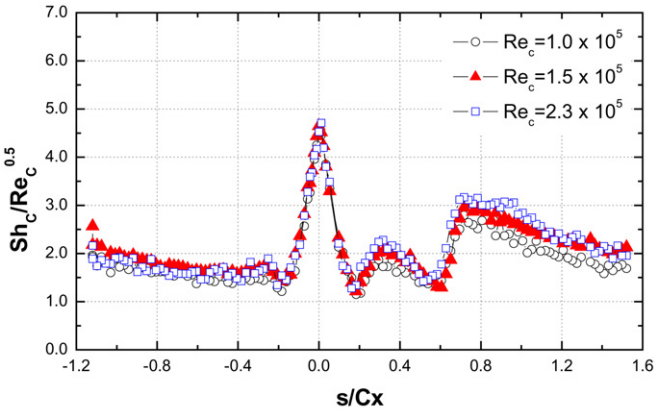

(a) $Sh_C/Re_C^{0.5}$

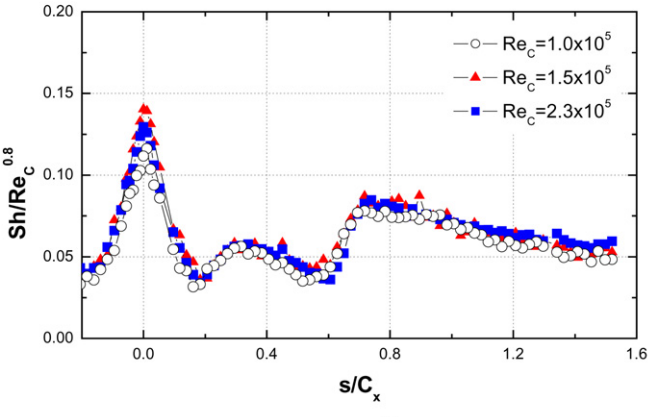

(b) $Sh_C/Re_C^{0.8}$

Fig. 14. Local distributions of normalized Sh_C along $z/C_x = 0.4$ for Position 5 at various Reynolds numbers. (a) Sh_C–$Re_C^{0.5}$, (b) Sh_C–$Re_C^{0.8}$.

due to variation in the flow condition. The heat transfer patterns on the near-tip surface of the blade are seriously affected because the behavior of the tip leakage flow changes with variation in blade position. The difference in heat/mass transfer coefficients near the tip is 30–50% of the average value However, the wake effect from the upstream guide plate is confined to the leading edge region possibly due to weak wake strength with flow acceleration.

Thus, the variation in the blade position causes heat transfer variations on the blade surface, especially the near-tip region. This might result in deterioration of durability in the tip region during actual operating conditions.

References

[1] P.H. Chen, R.J. Goldstein, Convective transport phenomena on the suction surface of a turbine blade including the influence of secondary flows near the endwall, ASME J. of Turbomachinery 114 (1992) 776–787.
[2] R.J. Goldstein, H.P. Wang, M.Y. Jabbari, The influence of secondary flows near the endwall and boundary layer disturbance on convective transport from a turbine blade, ASME Paper No. 94-GT-165, 1994.
[3] J.C. Han, L. Zhang, S. Ou, Influence of unsteady wake on heat transfer coefficient from a gas turbine blade, ASME J. of Heat Transfer 115 (1993) 904–911.
[4] T. Arts, J.-M. Duboue, G. Rollin, Aerothermal performance measurements and analysis of a two-dimensional high turning rotor blade, ASME J. of Turbomachinery 120 (1998) 494–499.
[5] M.F. Blair, An experimental study of heat transfer in a large-scale turbine rotor passage, ASME J. of Turbomachinery 116 (1994) 1–13.
[6] R.J. Goldstein, R.A. Spores, Turbulent transport on the endwall in the region between adjacent turbine blades, ASME J. of Heat Transfer 110 (1988) 862–869.
[7] K. Hermanson, S. Kern, G. Picker, S. Parneix, Predictions of external heat transfer for turbine vanes and blades with secondary flowfields, ASME J. of Turbomachinery 125 (2003) 107–113.
[8] P.W. Giel, R.J. Boyle, R. Bunker, Measurements and predictions of heat transfer on rotor blades in a transonic turbine cascade, ASME J. of Turbomachinery 126 (2004) 122–129.
[9] D.H. Rhee, H.H. Cho, Effect of vane/blade relative position on heat transfer characteristics in a stationary blade: Part 1. Tip and shroud, International Journal of Thermal Science 47 (11) (2008) 1528–1543.
[10] J.S. Kwak, J.C. Han, Heat transfer coefficients on the squealer tip and near squealer tip regions of a gas turbine blade, ASME J. of Heat Transfer 125 (2003) 669–677.
[11] P. Jin, R.J. Goldstein, Local mass/heat transfer on turbine blade near-tip surface, ASME J. of Turbomachinery 125 (2003) 521–528.
[12] H.G. Kwon, S.W. Lee, B.K. Park, Measurements of heat (mass) transfer coefficient on the surface of a turbine blade with a high turning angle using naphthalene sublimation technique, KSME Journal B 26 (2002) 1077–1087.
[13] D.H. Rhee, H.H. Cho, Local heat/mass transfer characteristics on a rotating blade with flat tip in a low speed annular cascade: Part 1. Near-tip surface, ASME J. of Turbomachinery 128 (2006) 96–109.
[14] D.H. Rhee, H.H. Cho, Local heat/mass transfer characteristics on rotating blade with flat tip in a low speed annular cascade: Part 1. Near-tip surface, ASME J. of Turbomachinery 128 (2006) 96–109.
[15] D.H. Rhee, H.H. Cho, Local heat/mass transfer characteristics on rotating blade with flat tip in a low speed annular cascade: Part 2. Tip and shroud, ASME J. of Turbomachinery 128 (2006) 110–119.
[16] L. Zhang, J.C. Han, Combined effect of free-stream turbulence and unsteady wake on heat transfer coefficients from a gas turbine blade, ASME J. of Heat Transfer 117 (1995) 296–302.
[17] H. Du, S. Ekkad, J.C. Han, Effect of unsteady wake with trailing edge coolant ejection on detailed heat transfer coefficient distributions for a gas turbine blade, ASME J. of Heat Transfer 119 (1997) 242–248.
[18] D.H. Rhee, H.H. Cho, Detailed heat transfer characteristics on rotating turbine blade, KSME Journal B 30 (2006) 1074–1083.
[19] R.J. Goldstein, H.H. Cho, A review of mass transfer measurement using naphthalene sublimation, Experimental Thermal and Fluid Science 10 (1995) 416–434.
[20] S.J. Kline, F. McClinetock, Describing uncertainty in single sample experiments, Mechanical Engineering 75 (1953) 3–8.
[21] E.R.G. Eckert, H. Sakamoto, T.W. Simon, The heat and mass transfer analogy factor, Nu/Sh, for boundary layers on turbine blade profiles, International Journal of Heat and Mass Transfer 44 (2001) 1223–1233.